Rock and Soil Mechanics

Volume 41 | Issue 5 Article 7

10-13-2020

Experimental study of single pile–soil interaction under horizontal low-cycle reciprocating displacement

Fu-yun HUANG
Fujian Key Laboratory of Engineering Structure, College of Civil Engineering, Fuzhou University, Fuzhou, Fujian 350108, China

Han-lun CHEN
Fuzhou Urban and Rural Construction Development Co. Ltd, Fuzhou, Fujian 350007, China, 546064617@qq.com

Rui DONG
Fujian Key Laboratory of Engineering Structure, College of Civil Engineering, Fuzhou University, Fuzhou, Fujian 350108, China

Yu-lin SHAN
Fujian Key Laboratory of Engineering Structure, College of Civil Engineering, Fuzhou University, Fuzhou, Fujian 350108, China

Custom Citation

HUANG Fu-yun, CHEN Han-lun, DONG Rui, SHAN Yu-lin, . Experimental study of single pile–soil interaction under horizontal low-cycle reciprocating displacement[J]. Rock and Soil Mechanics, 2020, 41(5): 1625-1634.

Rock and Soil Mechanics 2020 41(5): 1625–1634 ISSN 1000–7598
https: //doi.org/10.16285/j.rsm.2019.5723 rocksoilmech.researchcommons.org/journal

Experimental study of single pile–soil interaction under horizontal low-cycle reciprocating displacement

HUANG Fu-yun[1], CHEN Han-lun[1, 2], DONG Rui[1], SHAN Yu-lin[1]

1. Fujian Key Laboratory of Engineering Structure, College of Civil Engineering, Fuzhou University, Fuzhou, Fujian 350108, China

2. Fuzhou Urban and Rural Construction Development Co. Ltd, Fuzhou, Fujian 350007, China

Abstract: To ensure better horizontal deformation resistance, the pile foundation of integral abutment jointless bridges (IAJBs) should be designed as flexible pile. However, the calculation algorithm of flexible pile in relevant codes in China is mainly applied to the laterally loaded pile, and whether it can be used to identify the flexible pile for IAJBs remains a tricky issue to be studied. Therefore, in order to study the aseismic performance and interaction mechanism of the single pile–soil system, three concrete model piles with different lengths were tested under horizontal low-cycle reciprocating displacement based on a specially designed pile deformation measurement method. The result shows that the earliest cracking position of concrete pile is between 3–6 times of pile diameter. The deeper the pile is buried, the better the effect of pile–soil interaction with a deeper location of the deformation characteristic point. Meanwhile, stiffness of pile–soil system, horizontal ultimate bearing capacity and aseismic performance is improved with burial depth increased. The result also indicates that, when the pile–soil system reach the elastoplastic stage, the flexible performance of the pile will gradually degenerate from the elastic pile to the rigid pile. Furthermore, the provisions in relevant codes in China are not safe enough when evaluating the flexural performance of the pile foundation of integral abutment jointless bridges. Hence, it is recommended to use the Broms method for the benchmarking calculation in practical engineering.

Keywords: flexible pile; transverse stiffness coefficient; depth coefficient; flexural performance; horizontal reciprocating displacement

1 Introduction

Integral abutment jointless bridges (IAJBs) is a kind of bridge structure in which the superstructure is connected with the pile foundation of abutment. There is a typical structure-soil interaction (SSI) problem under the effect of temperature variation and concrete creep in engineering design. The abutment transfers the deformation of the superstructure to the pile so that it interacts with the soil under horizontal reciprocating displacement. Therefore, in order to ensure that the structure has a better resistance to horizontal deformation, the pile foundation should be designed as flexible pile [1]. In the *code for design of ground base and foundation of highway bridges and culverts* (JTG D63–2007)[2] and the *technical code for building pile foundations* (JGJ94–2008) [3], an algorithm to judge the working character of laterally loaded pile is provided. First, the transverse stiffness coefficient Q of pile–soil system (parameter reflecting the deformation capacity of the system (m)) is calculated. Then, the working characteristics of laterally loaded pile are judged by depth coefficient Z_Q (ratio of buried depth L_t to Q). Pile foundation belongs to rigid pile when $Z_Q < 2.5$, belongs to semi-rigid pile when $2.5 \leqslant Z_0 \leqslant 4.0$, and belongs to flexible pile when $Z_0 > 4.0$. This algorithm is mainly applied to laterally loaded pile [4], and whether it can be used to the whole bridge is still an important issue to be verified.

Previous studies have shown that obvious "disengaging" between pile and soil will appear when the pile top is subjected to horizontal reciprocating load or displacement[5–7]. With the change of horizontal displacement, the compacted degree and the comprehensive stiffness of pile–soil system will also change gradually [8–10], thus affecting the horizontal working behavior of piles. Through centrifugal model tests and 3-D finite element analysis, Hong et al. [11] found that with the increase in the number of reciprocating loads, the working characteristics of the pile–soil system gradually deteriorated from a flexible pile to a semi-rigid pile. Zhao et al. [12] found that, compared with one-way horizontal loaded piles, reciprocating horizontal loads would increase the response deformation of semi-rigid piles, which make the horizontal working characteristics of the system tend to be rigid piles by dynamic in-situ tests.

However, aforesaid researches only analyzed the

Received: 21 April 2019 Revised: 18 September 2019
This work was supported by the National Natural Science Foundation of China(51578161), Fujian New Century Talents Program(50011504) and the Project of Fuzhou Science and Technology (2018-G-63).
First author: HUANG fu-yun, male, born in 1979, PhD, Professor, Doctoral tutor, research interests: jointless bridges. E-mail: 52375495@qq.com
Corresponding: CHEN Han-lun, male, born in 1994, Master, specialized in the jointless bridges and basic engineering. E-mail: 546064617@qq.com

variation trend of single pile under horizontal reciprocating load or displacement qualitatively. Budhu et al[13] and Dobry et al.[14] carried out many in-situ tests and finite element analysis for single pile under horizontal reciprocating load in clay and sand, respectively. They suggested that the modulus ratio between pile and soil should be used as the basis for determining the working characteristics of single pile. However, this discrimination method ignored the important influencing factors such as the buried depth of pile foundation, pile diameter and boundary conditions. Broms[15] studied the working characteristics of single pile under horizontal dynamic load through a large number of laboratory model tests. Combining with parameter analysis, Broms proposed a calculation method (hereinafter referred to as Broms method).

Ashour et al. [16] presented deformation curves of 3 types of laterally loaded pile, as shown in Fig.1. When the horizontal deflection happens, there are at least two zero deformation points (i.e. S_{1a}, S_{2a}) and reversal deformation points (i.e. F_{1a}, F_{2a}) along the laterally loaded pile, as shown in Fig.1(a). In contrast, semi-rigid piles have only one zero deformation point (i.e. S_{1b}) and reversal deformation point (i.e. F_{1b}), as shown in Fig.1(b). When the rigid pile is deformed, there is only one deformation point S_{1c} and no deflection of the pile, which is shown in Fig.1(c), where $S_{1a} > S_{1b} > S_{1c}$, $F_{1a} > F_{1b}$. However, because the pile is buried in the soil, it is difficult to get the deformation curve of the pile, so the criterion based on the deformation characteristics of the pile cannot be directly applied to practical projects.

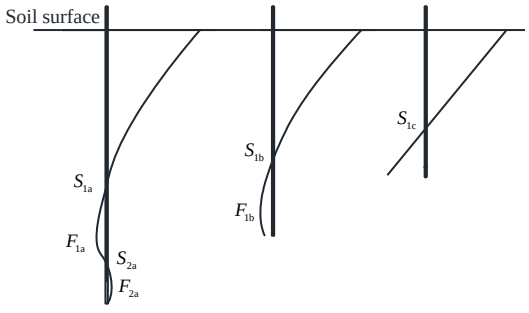

(a) Flexible pile (b) Semi-rigid pile (c) Rigid pile

Fig.1 Flexural performance of laterally loaded pile

Three concrete model piles with different lengths were tested under horizontal low-cycle reciprocating displacement. The test adopted a specially designed pile deformation measurement method which can measure the pile deformation under different reciprocating displacements[17]. Then comprehensive analysis of the interaction mechanism of pile–soil system under low lateral reciprocating displacement was made using the test data of system bearing capacity, pile strain and soil resistance. On the other hand, the variation trend of horizontal reciprocating displacement of single pile was determined based on the deformation characteristics of different model piles. Furthermore, the calculation methods for discriminating flexible pile in relevant specifications were preliminarily verified in this study.

2 Experimental scheme

2.1 Design of model piles

Three concrete model piles numbered RC-1, RC-2 and RC-3 were designed and made, respectively. The length L of specimen piles are 3.19 m, 3.50 m and 3.81 m, and pile diameter D is 155 mm. The top of the specimens is 0.3 m above the soil surface, and the buried depth is 2.89 m, 3.20 m and 3.51 m, respectively. The other parameters are listed in Table 1.

Table 1 Parameters of the model piles

Number	Reinforcement ratio/ %	Pile diameter D / mm	Pile length L /m	Buried depth L_t / m	L_t/d
RC-1	1.6	155	3.19	2.89	18.65
RC-2	1.6	155	3.50	3.20	20.65
RC-3	1.6	155	3.81	3.51	22.65

Flexible pile can be determined by the transverse stiffness coefficient Q_i (i=1–3) and depth coefficient Z_Q according to the algorithm proposed in the Codes[2–3] and Broms method[15], In the Codes, the transverse stiffness coefficient of pile foundation [2–3] is

$$Q_1 = \sqrt[5]{\frac{EI}{mb_0}} \tag{1}$$

where EI is the bending stiffness of pile and set as 834.33 kN·m^2 for all the 3 specimens; m is the foundation reaction coefficient; and b_0 is the width of the pile–soil system, and its calculation can refer to literatures 2 and 3.

In Broms method, the transverse stiffness coefficient is calculated by [15]

$$Q_2 = \sqrt[5]{\frac{EI}{n_k}} \tag{2}$$

where n_k is the modulus constant of foundation reaction, according to the material parameters of used soil in section 2.2, m and n_k are set as 10 MN/m^4 and 3 MN/m^3 by Table 5.7.5 in the code[3] and Table 7 in literature [15], respectively; b_0 is 0.66 m for all the

https://rocksoilmech.researchcommons.org/journal/vol41/iss5/7
DOI: 10.16285/j.rsm.2019.5723

three specimens, which is calculated by formula $b_0 = 0.9(1.5D + 0.5)$.

The depth coefficients Z_Q of the specimens can be caculated by

$$Z_Q = L_t / Q_i \quad (3)$$

After Q_i and Z_{Q_i} are obtained by Eqs.(1)–(3), the horizontal working characteristics of the specimens can be determined in terms of the criteria in Table 2. Based on the algorithm in *technical code for building pile foundations* [3], all the specimens belong to flexible piles according to Table 2. However, this results are different form the ones determined by Broms method (i.e. RC-1 is a semi-rigid pile, specimens RC-2 and RC-3 are flexible piles).

Table 2 Identification of working characteristics of the model piles

Index	Algorithm	Q_i /m	Z_{Q_i}	The range of flexible pile	Working characteristics
RC-1	Codes[2-3]	0.66	4.38	$Z_{Q_i} > 4.0$	flexible pile
	Broms method	0.77	3.73		semi-rigid pile
RC-2	Codes[2-3]	0.66	4.84	$Z_{Q_i} > 4.0$	flexible pile
	Broms method	0.77	4.13		flexible pile
RC-3	Codes[2-3]	0.66	5.30	$Z_{Q_i} > 4.0$	flexible pile
	Broms method	0.77	4.52		flexible pile

2.2 Materials quality testing

The concrete of the specimen pile was tested on the basis of the provisions of the *standard for test and evaluation of concrete compression strength* (GB/T 50107-2010) [18].

The test results show that, for concrete cube, the compressive strength of the 28 d is 47.6 MPa, the elastic modulus is 3.25×10^4 MPa, the Poisson's ratio is 0.195, and the density is 2.40 g/cm^3. For longitudinal reinforcement, the measured yield strength of the specimens is 337MPa, the ultimate tensile strength is 454 MPa, and the elastic modulus is 2.00×10^5 MPa. The yield strength of stirrup is 302 MPa, the ultimate tensile strength is 424 MPa, and the elastic modulus is 2.10×10^5 MPa.

Minjiang River sand from Fujian province was selected as the test soil in this study. According to the *Code for investigation of geotechnical engineering* (GB50021-2001)[19], the measured material parameters are listed in Table 3, belonging to medium coarse sand with medium-density.

Table 3 Soil parameters of Minjiang River sand

Water content w / %	Density / (g • cm^{-3})	Void ratio e	Internal friction angle φ / (°)	Compression modulus / MPa	Average SPT N	Relative compactness / %
0.8	1.50	0.80	35.86	28.9	11	53

2.3 Test soil box

A large volume soil box with a size of 2m×3m×4m was used in this test, as shown in Fig. 2(a). The model piles were buried in the center of the soil box, and the distance from the pile to the wall of the box can satisfy the requirements of boundary conditions so that the influence of the boundary effect on the test results could be ignored.

2.4 Arrangement of measuring points

On the basis of the arrangement method in literatures [10,17], 13 displacement meters were arranged along the pile, as shown in Fig.2(b). 14 subminiature pressure cells were symmetrically pasted on the surface of the pile with hot melt adhesive, 20 resistance strain gauges were pasted on the surface of the pile body with thin epoxy resin adhesive symmetrically, and the strain gauge surface was coated with thin wax waterproof. Due to the different lengths of specimens, the buried depth of each measuring point is slightly different. The buried depth of each measuring instrument relative to the soil surface is shown in Fig. 3.

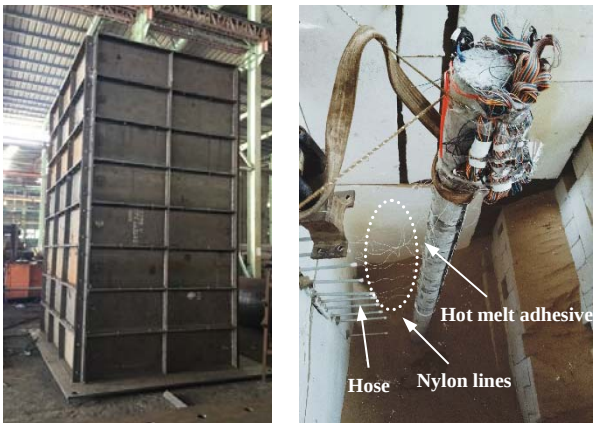

(a) Soil box (b) Inside view

Fig.2 Diagram of Experimental installation

2.5 Preparation and loading

This experiment was carried out in the key laboratory of engineering structure of Fuzhou University. Before the test, the model piles with the measuring meter/gauge/cell were first hoisted into the soil box and positioned, and sand was added into the box and compacted every 0.25 m until the design requirements were met.

The MTS actuator was used to impose a low cyclic reciprocating displacement, and the acting point of the actuator was about 0.15 m above the soil surface. Low loading rate (i.e. 1.0 mm/s) was used to reset shift, which was classified as low-cycle reciprocating loading [4], so the change of stress and strain caused by

loading rate can be basically ignored here. Horizontal reciprocating displacements were applied at 2, 5, 8 and 10 mm successively before initial cracking, as shown in Fig.4(a). Within the range of 10–30 mm, the displacement of each stage was increased by 5 mm; after exceeding 30 mm, the displacement increment of each stage was 10 mm. If the bearing capacity of the pile droped below 0.85 times the ultimate bearing capacity under the application of a certain displacement, the pile was deemed to have failed, and loading should be stopped immediately. The displacement cycle was repeated three times for each stage. After 0.5min of load holding, the data of measuring point was collected and the disengaging was recorded. The complete displacement loading history is presented in Fig. 4(b).

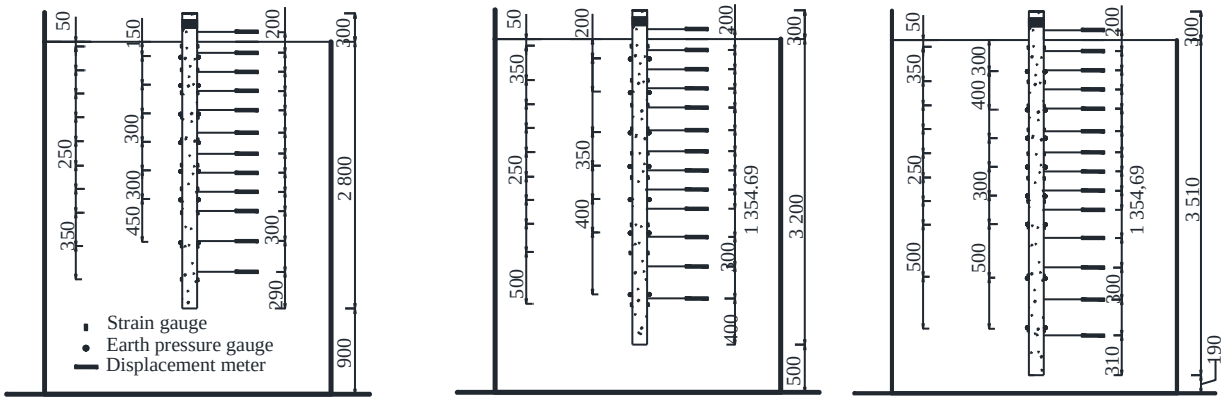

(a) RC-1 (b) RC-2 (c) RC-3

Fig.3 Arrangement of measuring points (unit: mm)

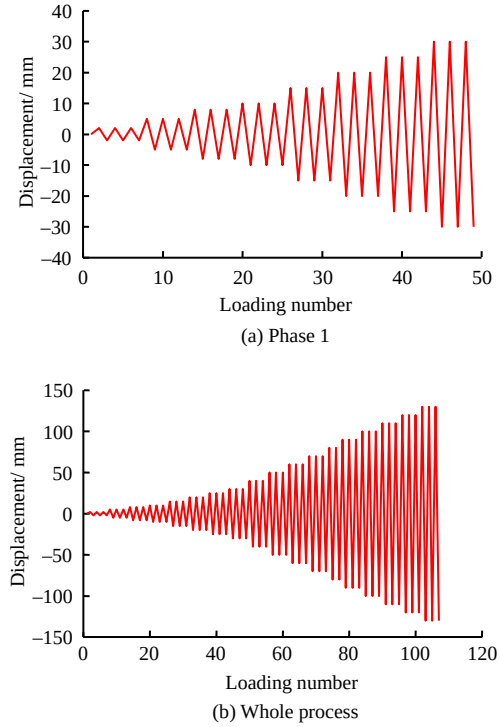

(a) Phase 1

(b) Whole process

Fig.4 Displacement loading history

3 Analysis of experimental results

3.1 Destruction characteristics of the model piles

The destruction of the model piles is shown in Fig. 5. All the three specimens produced 4 cracks, which are distributed in the buried depth range of 3*D*-6*D*, with the spacing of about 1*D*. The failure location of specimen RC-3 is the deepest (buried depth is 4.32*D*), followed by RC-2 (buried depth is 4.22*D*), and RC-1 is the shallowest (buried depth is 4.03*D*). It can be summarized that, under the same other conditions, the deeper the pile foundation is buried, the deeper the pile side soil can participate in the pile–soil interaction, and the better the interaction effect is.

(a) RC-1 (b) RC-2 (c) RC-3

Fig.5 Destruction of the model piles

3.2 Skeleton curves

Figure 6 illustrates the skeleton curves of three concrete model piles. Their forces and displacements were collected and recorded by the acquisition system built into the MTS actuator. According to the skeleton diagram, the whole process of concrete single pile–soil interaction under horizontal reciprocating displacement can be divided into four stages: elastic (*OA*), elastoplastic (*AB*), plastic (*BC*) and failure (*CC'*). Due to

space limitations, the following analysis is mainly carried out with RC-3 as an example.

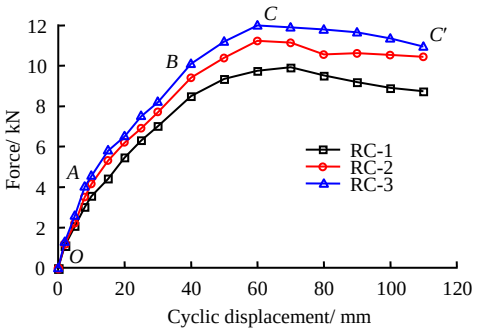

Fig.6 Skeleton curves of model piles

Figure 6 shows that when the reciprocating displacement is less than 10 mm, RC-3 is in the elastic stage. Point *A* is the cracking point of concrete pile, the elastic limit displacement y_{cr} and elastic limit load F_{cr} are 10 mm and 0.412 kN, respectively, and the corresponding elastic flexural rigidity K_{cr} is 0.412 kN/mm. Compared with RC-3, the F_{cr} values of the other two piles decreased by 6% and 15%. However, the elastic flexural rigidity of the three model piles is basically the same, the value of which is around 0.4 kN /mm.

When the reciprocating displacement is over 10 mm, RC-3 enters the elastic-plastic stage, and the slope of skeleton curve gradually decreases. Explicitly, cracks appear on the pile shaft, and the deformation capacity is improved at this stage. Point *B* is the yield limit, the yield displacement and yield load are 40 mm and 10.10 kN,respectively. The corresponding yield bending stiffness is 0.25 kN /mm. In contrast, the yield bending stiffness of RC-2 and RC-1 decreased by 13% and 24% to 0.23 and 0.21 kN/mm.

When the reciprocating displacement exceeds 40mm, the model pile RC-3 enters the plastic stage, and the slope of skeleton curve continues to decrease. At this stage, the concrete in compression zone of model pile reaches the compression limit, and the external load is mainly borne by the pile side soil. Further, when the pile side soil also reaches the compression limit, the pile–soil system cannot continue to bear greater external load, as shown in Fig. 6, point *C*. At this point, the plastic ultimate displacement y_u and ultimate load F_u are 60 mm and 12.11kN, respectively, and the plastic bending stiffness is 0.20kN/mm. Compared with the previous stage, the plastic bending stiffness of RC-2 and RC-1 decreased by 5% and 43% to 0.19 and 0.14 kN/mm, respectively. Therefore, the deeper the pile foundation is buried, the greater the flexural rigidity of the pile–soil system and the higher the horizontal ultimate bearing capacity are.

When the reciprocating displacement is greater than 60 mm, the bearing capacity of pile–soil system begins to decline. When the reciprocating displacement is 110 mm，the bearing capacity drops to about 85% of the ultimate bearing capacity F_u, hence 110 mm can be used as the limit displacement of the model piles, as shown in Fig. 6, point C'.

3.3 Deformation of the model piles

3.3.1 Elastic stage

Figure 7(a) shows the pile deformation curve of RC-1 at the elastic stage. The pile deformation curve of RC-1 only has one zero deformation point S_{RC-1} and one reversal deformation point F_{RC-1}. The horizontal working behavior of RC-1 is more similar to that of semi-rigid pile, but inconsistent with the discriminant result given by "Code"[2–3]. Therefore, the estimated results may be unsafe if the algorithm proposed in the Codes is used to identify the flexible pile under horizontal reciprocating displacement.

Figure 7(b) illustrates the comparison of deformation curves of 3 model piles under 5 mm reciprocating displacement. At the elastic stage, there are two zero deformation points (i.e. S_1, S_2) in the deformation curves of piles RC-2 and RC-3, and the horizontal working behavior is more similar to that of flexible pile, which is consistent with the discrimination results given by "Code" and Broms method. The dotted line in Fig.7(b) is the tangent line at the zero deformation point. Smaller the angle between the tangent line and the original pile position is, the greater the degree of pile deflection will be. The deformation curves of model piles RC-1, RC-2 and RC-3 correspond to angles of 32.17°, 23.90° and 19.27°, respectively. Therefore, the deeper the pile is buried, the greater the degree of deflection and flexibility of the pile will be.

3.3.2 Inelastic stage

Figures 7(c) and 7(d) show the deformation characteristic points (i.e. S_1, F_1) of the three model piles and the curves which change with the loading displacement, where, point S_1 is the intersection point of the deformation curve and the position of the original pile. At the elastic stage, the deformation feature points of the model piles basically remain unchanged. The curves of different model piles indicate that the deeper the piles are buried, the deeper the deformation feature points are.

In addition, the Code[2–3] stipulates that the horizontal working behavior of pile foundation is rigid pile when $Z_Q < 2.5$. For the specimens in this test, the pile

foundation is rigid when the buried depth is less than 11*D*. As shown in Fig.7(d), when the reciprocating displacement is greater than 50 mm, the points F_1 of the three deformation curves will fall into the buried depth range of 10*D*. Thus, it can be considered that after the pile–soil system enters the plastic stage, the working characteristics of the specimen gradually degenerate to the rigid pile. With the increase of reciprocating dis- placement and the increase of reciprocating times, the horizontal working behavior of pile foundation will gradually degenerate and finally degenerate into a rigid pile.

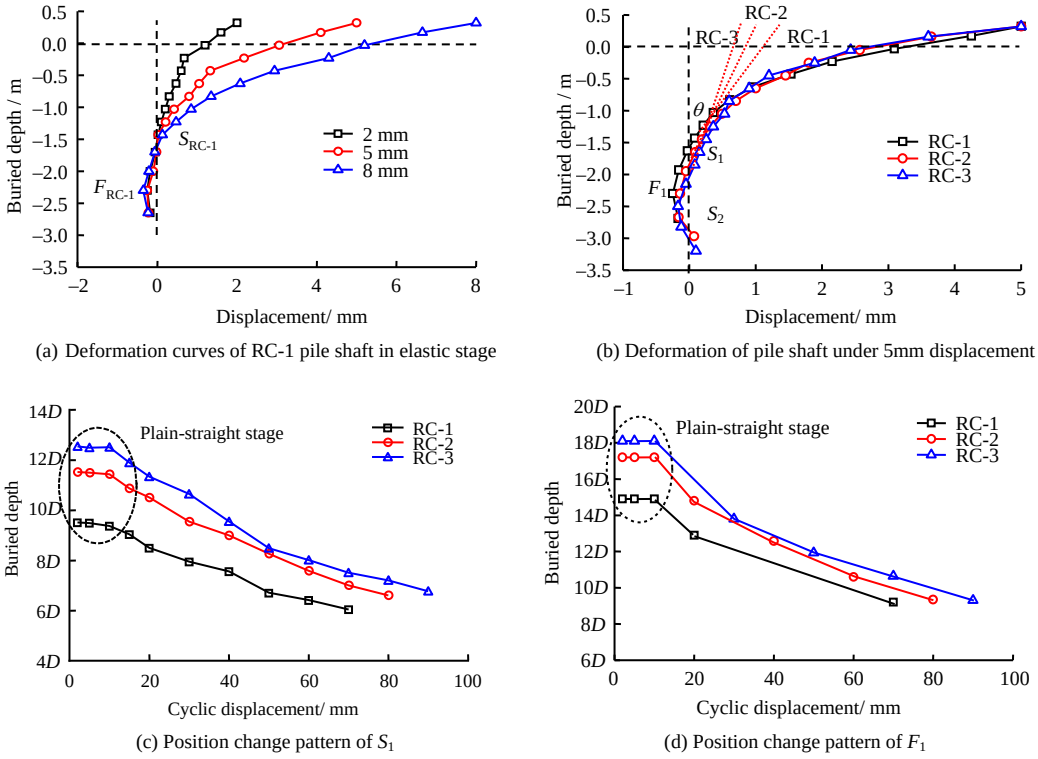

(a) Deformation curves of RC-1 pile shaft in elastic stage

(b) Deformation of pile shaft under 5mm displacement

(c) Position change pattern of S_1

(d) Position change pattern of F_1

Fig.7 Deformation of the model piles

3.4 Strain of the pile shaft

Considering that the pile strain curves of the three specimens have similar variation rules, Figure 8 shows the pile strain curves, tensile and compressive strain histories of the specimen RC-3, respectively, and take RC-3 as the typical analysis.

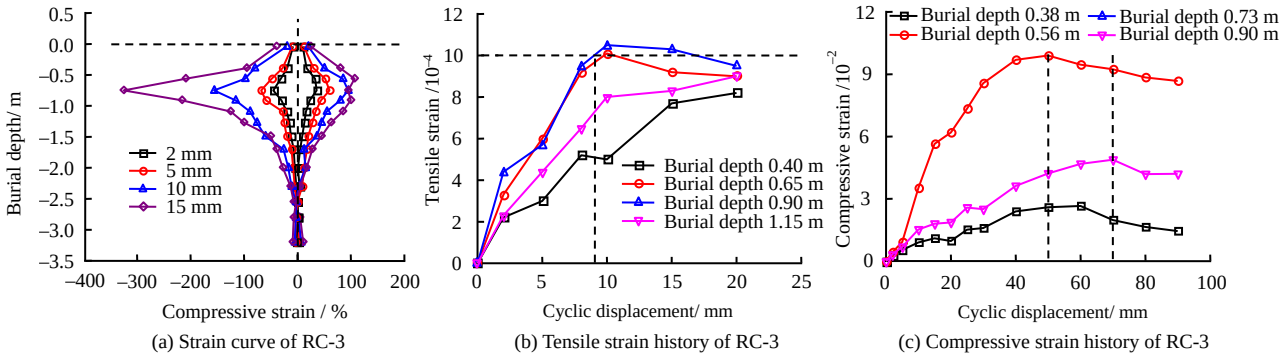

(a) Strain curve of RC-3

(b) Tensile strain history of RC-3

(c) Compressive strain history of RC-3

Fig.8 Strain along the model pile shaft

According to Fig. 8(a), it is found that, when the reciprocating displacement is less than 10 mm, the strain curves of specimen RC-3 are symmetric; when the reciprocating displacement is greater than 10 mm, the tensile and compressive strains of the pile are no longer symmetrical. Under the reciprocating displacement of 10 mm, the maximum compressive strain of RC-3 reaches 1.63×10^{-4}, while the tensile strain remains at about 1.00×10^{-4}. Since the ultimate tensile strain of C40 concrete is about 1.00×10^{-4}, the reciprocating displacement of 10 mm can be regarded as the cracking displacement of pile concrete from the perspective

of pile strain. Accordingly, the cracking displacements of the model piles RC-1 and RC-2 are 10 mm and 8mm, respectively. Increasing the buried depth can improve the anti-crack performance of pile–soil system, that is, the anti-crack ability of flexible pile is better than that of semi-rigid pile. Due to the spacing between the positions of the strain sensors, the position and magnitude of the maximum strain of the pile cannot be accurately obtained. However, from the change trend of the curve, the larger tensile and compressive strain of the specimen RC-3 appear within the buried depth of 3*D*-6*D*, which is consistent with the range of pile cracking.

Figures 8(b) and 8(c) illustrate the tensile and compressive strain history curves of model pile RC-3 respectively, which can preliminarily manifest the trend of pile–soil bearing ratio in the loading process. When the reciprocating displacement is small, the pile strain of RC-3 increases rapidly. At this case, the pile has not cracked and can bear a higher proportion of external load. When the reciprocating displacement exceeds the elastic limit, the compressive strain of RC-3 at the buried depth of 0.73 m exceeds the range of sensor rapidly. The strain sensor may be damaged prematurely due to pile cracking or wire breakage of sensor. Except for the measuring points at this location, the pile compressive strain at other measuring points of specimen RC-3 continues to increase at a faster speed. Although the pile has cracked, it can still bear more loads in this instance. However, with the redistribution of pile stress, more soil is involved in the pile–soil system, and the bearing ratio of soil is increased, which make the bearing ratio of pile decreases at this stage.

When the reciprocating displacement reaches the yield limit, the compressive strain of the pile cannot continue to increase, that is, when the concrete in the compression zone of the pile also reaches the compression limit, the maximum compressive strain of the pile of specimen RC-3 reaches 1.035×10^{-3}, and the ultimate compressive strains of specimens RC-2 and RC-1 are 1.019×10^{-3} and 8.98×10^{-4}, respectively. According to the analysis of skeleton curve in Section 3.2 of this paper, the plastic limit displacement of model pile RC-3 is 60 mm. As shown in Fig.8(c), when the compressive strain of model pile RC-3 reaches the limit value, the corresponding reciprocating displacement is 50 mm, which is less than the plastic limit displacement. The plastic limit dislocations of RC-2 and RC-1 are 60 mm and 70 mm, respectively, but the corresponding reciprocating displacements when the pile compressive strain reaches the limit value are also 50 mm. It implies that the horizontal bearing capacity of the pile–soil system can continue to increase when the concrete in the compression zone of the pile is damaged, and the soil is still in the bearing state.

When the reciprocating displacement exceeds the limit value, the maximum compressive strain of specimen RC-3 decreases. When the reciprocating displacement reaches 70 mm, the pressure strain of other buried piles also begins to decrease. The pile compressive strain curves of specimen RC-2 and RC-1 also show the same trend. Therefore, the deflection degree of pile decreases gradually when the reciprocating displacement exceeds the plastic limit. From the point of view of laterally loaded pile performance, rigid pile mainly rotates around the point S_1 of the pile deformation curve when it bears horizontal load. It indicates that the deformation characteristics of pile gradually approaches the rigid pile after the reciprocating displacement exceeds the plastic limit. With the increase of reciprocating displacement and the increase of reciprocating number, the horizontal working behavior of a single pile will gradually degenerate to the rigid pile, which is consistent with the analysis results in Section 3.3 in this paper.

3.5 Pile bending moment

3.5.1 Calculation of bending moment

When the pile–soil system is in an elastic stage, the bending moment *M* of the model pile is

$$M=\frac{EI(\varepsilon_{\mathrm{t}}-\varepsilon_{\mathrm{c}})}{D} \tag{4}$$

where ε_{t} is the measured value of tensile strain; ε_{c} is the measured value of compressive strain.

The comparison of cracking bending moments of model pile shaft is illustrated in Fig. 9.

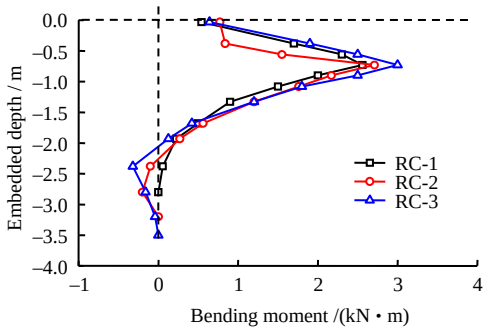

Fig.9 Comparison of pile bending moments

In the elastic stage, the maximum bending moment of model pile is located at the buried depth of 4.2*D*, which is consistent with the actual failure position of

the pile. The corresponding cracking bending moments are 2.6 kN·m, 2.8kN·m and 3.2kN·m, respectively. It indicates that the deeper piles embedded have greater bending moment.

3.5.2 Trend of pile–soil bearing ratio

This section will further analyze the variation trend of pile–soil bearing ratio from the perspective of bending moment change along the pile shaft. In the pile–soil interaction system, the bending moment of pile is provided by external load, the soil around the pile and the pile itself. Assuming that the measured bending moment is M_{T}, the bending moment of pile without soil resistance is M_{L}, and the bending moment caused by soil resistance is M_{S}, as shown in Fig. 10(a).

Bending moment of pile without soil resistance M_{L} and bearing ratio of pile γ_{p} are given as

$$M_{\mathrm{L}} = M_{\mathrm{T}} + M_{\mathrm{S}} \tag{5}$$

$$\gamma_{\mathrm{p}} = M_{\mathrm{T}} / M_{\mathrm{L}} \tag{6}$$

Although the bearing ratio of pile calculated by Eq. (6) is not accurate, the changing trend of the bearing ratio of pile–soil system can be qualitatively analyzed with γ_{p}, as shown in Fig. 10(b).

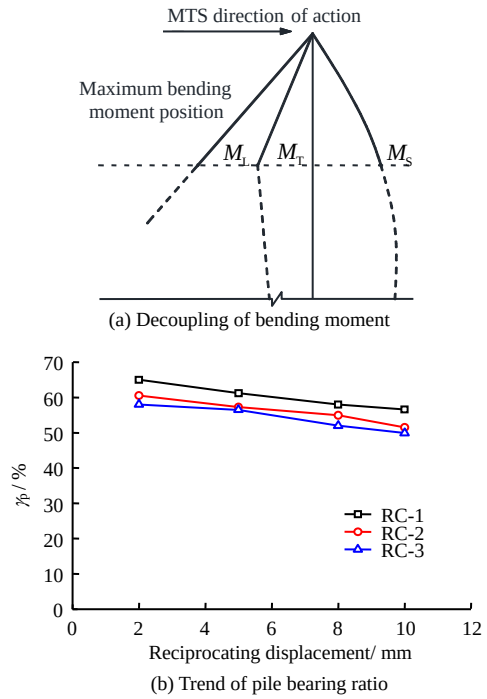

Fig.10 Trend of pile–soil bearing ratio

As illustrate in Fig. 10(b), when the reciprocating displacement is 2 mm, the γ_{p} values of model piles RC-1, RC-2 and RC-3 are 65.21%, 60.85% and 57.92%, respectively. When the reciprocating displacement is less than 8mm, the values of γ_{p} decrease, but it is also more than 50%. It can be indicated that in the elastic stage, the pile bears a large proportion of load, and the mechanical properties of the pile will have a great impact on the pile–soil system. When the pile cracks, the γ_{p} values of three piles decrease to 59.74%, 53.85% and 52.18%, respectively. It can be summarized that a deeper installed pile leads to a smaller bearing ratio of pile shaft, and a closer the pile–soil interaction. In other words, the effect of flexible pile–soil interaction is better than that of semi-rigid pile.

In addition, under the same horizontal load, the deeper buried pile has a higher bearing ratio of pile side soil. Thus, the soil on the side of the pile bears more external load, which increases the displacement resulting the pile to crack. It is also consistent with the conclusion based on the analysis result of pile strain in Section 3.4.

3.6 Resistance of pile side soil

It can be observed from Fig.11(a) that the maximum soil resistance of model pile RC-3 appears around the buried depth of 0.8 m, slightly deeper than the position with the most serious pile damage (4.0*D*).When the buried depth of the pile is greater than 0.8 m, the greater the buried depth is, the less resistance of soil on the side of the pile is, and the decreasing trend gradually increases. Until a certain depth, the pile side soil resistance becomes negative, that is, the reverse pile deformation has occurred at that position. It can be summarized that the distribution of soil resistance on the pile side is consistent with the deformation of the pile shaft. The greater the deformation of the pile body, the greater the soil resistance on the pile side will be. The resistance of pile side soil is also related to the buried depth. When the pile is buried shallowly, the pile deformation is the largest, but the resistance of soil on the side of the pile is relatively small. Because the soil layer is thinner, the soil soon reaches its compression limit state. As a result, the soil cannot provide greater soil resistance. At the same time, with the increase of reciprocating displacement, there will be a certain degree of disengaging between pile and soil. The disengaging of pile–soil system makes the soil layer thickness in shallow position decrease gradually, which affects the distribution of soil resistance. When the reciprocating displacement exceeds 15 mm, the resistance of soil on the side of pile at the measuring point with a shallow buried depth decreases with the increase of pile deformation. When the reciprocating displacement transcends 20–25 mm, the maximum soil resistance of pile side of specimen RC-3 reaches 121 kPa, and those of specimen RC-2 and RC-1 reach 110kPa and 104kPa, respectively. According to the reference [10], 100kPa

is close to the limit of passive soil pressure of sand at that certain buried depth.

Figure 11(b) shows the curves of soil resistance caused by "circumfluence" of soil on the non-resistance side of specimen RC-3. It can be found that, when the reciprocating displacement surpasses 2 mm, the increasing of reciprocating displacement leads to a slight increase of the soil resistance on the non-resistance side, but the increment is almost negligible. The main reason is that the soil resistance on the non-resistance of the pile is mainly generated by the “circumfluence” of the soil around the pile. Due to pile shaft deformation, the soil in front of the pile is squeezed to the back side of the pile, thereby a certain amount of soil resistance can be measured.

By recording the active earth pressure of the pile side soil when the displacement of pile top is 0, it is found that the active earth pressure on the pile side will change with the increase of reciprocating displacement on the top of pile. However, the active earth pressure on the bearing side and the non-resistance side of the pile basically counteract each other, so the influence of the active earth pressure on the total resistance on the pile side can be ignored.

Figure 11(c) illustrates the comparison of soil resistance on the stressed side of three piles under the reciprocating displacement of 8 mm. As shown in the figure, the buried depth of pile is directly proportional to the total resistance of pile side. The greater the buried depth of pile, the closer the interaction between pile and soil is, and the higher the bearing ratio of soil in the pile–soil interaction is, which is consistent with the analysis results in Section 3.5.

3.7 Hysteretic curves of the model piles

It can be obtained from Fig. 12(c) that the hysteresis loop of specimen RC-3 develops from an inverse S-shape to an arch shape and then to a spindle shape, that is, the larger the reciprocating displacement is, the fuller the hysteresis loop will be, and the stronger the energy dissipation capacity of the system will be.

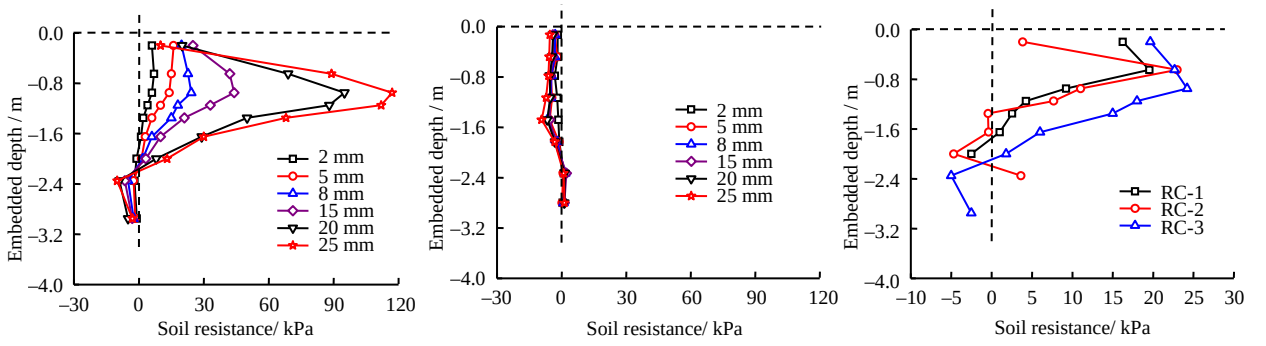

(a) Soil resistance on stressed side of RC-3 (b) Soil resistance on non-resistance side of RC-3 (c) Comparison of soil resistance on stressed side

Fig.11 Resistance curves of pile side soil

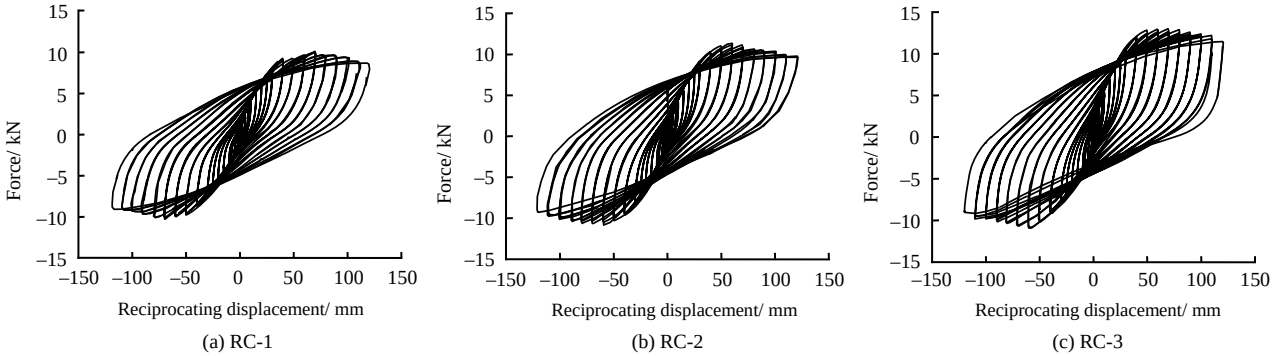

(a) RC-1 (b) RC-2 (c) RC-3

Fig.12 Hysteretic curves

Figure 12 also shows that the hysteresis fullness of specimen RC-3 is the highest, followed by specimen RC-2 and specimen RC-1. It can be summarized from the comparison that the energy dissipation capacity of flexible pile is more advantageous than that of semi-rigid pile, and the deeper the pile is buried, the stronger the energy dissipation capacity of pile–soil system is. The main reasons are as follows: a deeper buried pile foundation leads to a closer interaction of the pile–soil system and a higher bearing ratio of soil; and the better energy dissipation capacity of soil results in the better seismic performance.

4 Conclusion

Through the analysis and comparison of the results of the quasi-static tests, the following conclusions are

obtained:

(1) Under horizontal reciprocating displacement load, the interaction between concrete foundation pile and soil can be divided into four stages: elastic, elastoplastic, plastic and destructive. With the increase of reciprocating displacement, the initial crack position of pile is usually within the range of 4.0*D*–4.5*D* buried depth, and the corresponding crack dis- placement is 8–10mm. The positions of the maximum bending moment of pile, the maximum soil resistance of pile side and plastic deformation are all consistent with the failure position of pile. When the reciprocating displacement is greater than the elastic limit, the bearing ratio of pile, the position of deformation characteristic points and the comprehensive stiffness of pile–soil system will gradually deteriorate at the same time.

(2) The tests results shows that the deeper the pile is buried, the better the effect of pile–soil interaction with a deeper location of the deformation characteristic point. Meanwhile, stiffness of pile–soil system, horizontal ultimate bearing capacity and aseismic performance are improved with increasing burial depth.

(3) The comprehensive analysis of bearing capacity and deformation of pile–soil system illustrates that the horizontal working behavior of specimen RC-1 is more similar to that of semi-rigid pile, and the horizontal working behaviors of specimen RC-2 and RC-3 are more similar to that of flexible pile. If the algorithm recommended in Chinese codes[2–3] is used to identify the flexible pile, the result is not safe. In addition, with the increase of reciprocating displacement, the horizontal working behavior of single pile will gradually degenerate from flexible pile to rigid pile.

Due to the space limitation, this paper does not further give a method for determining the flexible pile suitable for IAJBs. It is suggested to refer to Broms method [15] for calculation in practical engineering.

Reference

[1] CHEN Bao-chun, ZHUANG Yi-zhou, HUANG Fu-yun, et al. Jiontless bridge[M]. Beijing: People's Transportation Publishing Press, 2019.

[2] China Communications Highway Planning and Design Institute Co., Ltd. JTG D63–2007. Code for design of ground base and foundation of highway bridges and culverts[S]. Beijing: People's Transportation Publishing Press, 2007.

[3] Ministry of Housing and Urban-Rural Development of the People's Republic of China. JGJ94–2008. Technical code for building pile foundation[S]. Beijing: China Construction Industry Publishing, 2008.

[4] Pile Foundation Manual Editing Committee. Pile foundation manual[M]. Beijing: China Construction Industry Press, 1995: 225–271.

[5] BEN H, LI Z W, YI H. Field testing of one-way and two-way cyclic lateral responses of single and jet-grouting reinforced piles in soft clay[J]. Acta Geotechnica, 2017, 12(5): 1–14.

[6] HUSSIEN M N, TOBITA T, IAI S, et al. Soil-pile separation effect on the performance of a pile group under static and dynamic lateral loads[J]. Canadian Geotechnical Journal, 2010, 47(11): 1234–1246.

[7] MAHESHWARI B, WATANABE H. Nonlinear dynamic behavior of pile foundations: effects of separation at the soil-pile interface[J]. Soils and Foundations, 2006, 46(4): 437–448.

[8] OGHABI P. Experimental response of a pile in sand under static and cyclic lateral loads[D]. Toronto: Queen's University, 2014.

[9] LEBLANC C, HOULSBY G, BYRNE B. Response of stiff piles in sand to long-term cyclic lateral loading[J]. Géotechnique, 2010, 60(2): 79–90.

[10] ZHUANG Yi-zhou, HUANG Fu-yun, QIAN Hai-min. Pseudo-static test research on mechanic behavior of PHC piles with pile–soil interaction[J]. China Journal of Highways, 2017, 30(4): 42–51.

[11] HONG Y, HE B, WANG L. Cyclic lateral response and failure mechanisms of a semi-rigid pile in soft clay: centrifuge tests and numerical modelling[J]. Canadian Geotechnical Journal, 2017: 339–356.

[12] ZHAO S, WANG T, WANG W. Experiment research and numerical simulation on dynamic characteristics of semi-stiff pile composite foundation[C]//International Conference on Electric Technology & Civil Engineering. Lushan: Jiangxi Lushan Publishing Press, 2011: 1109–1120.

[13] BUDHU M, DAVIES T. Analysis of laterally loaded piles in soft clays[J]. Geoenvironmental Engineering, 1988, 114(1): 21-39.

[14] DOBRY R, VICENTE E, ROURKE O, et al. Horizontal stiffness and damping of single piles[J]. Journal of Geotechnical and Geoenvironmental Engineering, 1982, 108(3): 71–79.

[15] BROMS B. Lateral resistance of pile in cohesionless soil[J]. Journal of Soil Mechanics Foundation Division, ASCE, 1964, 90(3):123–156.

[16] ASHOUR M, NORRIS G M. Laterally and axially loaded deep foundation systems computer program DFSAP final report[R]. Washington: Washington State Department of Transportation, 2006.

[17] HUANG Fu-yun, LIN You-wei. The utility model relates to a construction and installation method for accurately measuring the deformation of structures in soil: China, CN108007423A[P]. 2018.

[18] Ministry of Urban and Rural Construction and Environmental Protection of the People's Republic of China. GB/T 50107–2010. Standard for test and evaluation of concrete compression strength[S]. Beijing: China Building Industry Press, 2010.

[19] Ministry of Construction Comprehensive Survey, Research and Design Institute. GB50021–2001. Code for investigation of geotechnical engineering[S]. Beijing: China Building Industry Press, 2010.